Luminescence Properties and ROS Generation of Magnetic Porous Silicon Nanoparticles

Paula Caregnato[a*], Pedro M. David Gara[b], Eduardo D. Prieto[a], Mónica C. Gonzalez[a]

[a]Instituto de Investigaciones Fisicoquímicas Teóricas y Aplicadas (INIFTA), CCT—La Plata-CONICET, Universidad Nacional de La Plata, C.C. 16, Suc. 4, (1900) La Plata, Argentina.

[b]Centro de Investigaciones Ópticas (CIOP—CONICET—CIC) Universidad Nacional de La Plata, C.C. 3 (1897) Gonnet –Buenos Aires, Argentina.

* Corresponding author.
E-mail: caregnato@inifta.unlp.edu.ar
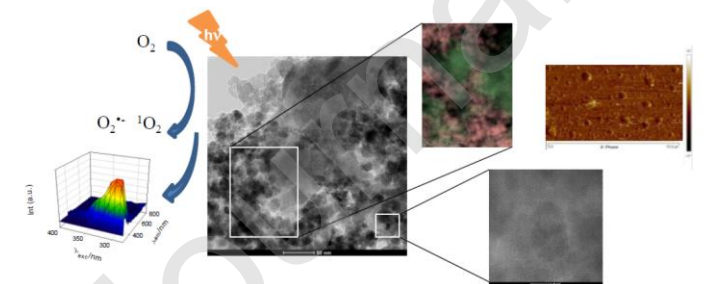Tel: --54 221 4257430/ 7291.Fax: --54 221 4254642

Others authors:

pedrodg@ciop.unlp.edu.ar
edprieto@quimica.unlp.edu.ar
mcgonzalez.quim@gmail.com

Graphical Abstract

Abstract

Magnetite–Porous Silicon 100-150 nm size nanoparticles (MPSi) were obtained combining luminescent and magnetic properties from silicon and magnetite, respectively.
MPSi hybrids were characterized by high-resolution transmission electron microscopy, atomic and magnetic force microscopy and X-ray photoelectron spectroscopy.

The presence of magnetite quenches statically visible luminescence of Porous Silicon toluene suspensions. Whereas MPSi, maintain the luminescence in the 300-450 nm spectral region.

Particles retained the capacity for singlet oxygen and superoxide radical ion generation (Reactive Oxygen Species, ROS). However quantum yield singlet oxygen generation is much lower than the PSi analogues and superoxide radical ion concentration dismiss when magnetite is incorporated in the PSi matrix.

Silanization of Porous Silicon and MPSi yield nanoparticles with −SH terminal groups with unique luminescence properties.

Keywords

Porous Silicon; Magnetite; Luminescence emission; ROS generation

1. Introduction

In the last years, Porous Silicon nanoparticles (PSi) are receiving increasing attention from the scientific biomedical population.

Unique physicochemical properties of PSi, for instance biocompatibility, high surface to volume ratio, customized surface stoichiometry, and simple surface functionalization, provide a potential material for controlled drug delivery, photodynamic therapy and bio-imaging (Airaksinen et al. 2014). Stable photoluminescence band of PSi in the visible region makes them excellent candidates for the development of photoluminescence–based biosensors (Myndrul et al. 2018). Moreover, silicon nanoparticles are nontoxic and thus, which dismiss environmental impact.

Actually, there are a large availability of techniques for the production and characterization of nanometric materials with controlled composition and shapes. Developing modifications to the nanostructures may improve their integration with biological media and reach the target tissue, leading to enhanced solubility, compatibility and recognition (Martin-Palma 2010).

In particular, Silicon nanomaterials combined with magnetic nanoparticles, allows a hybrid nanosctructure with unique set of properties such as the tunable luminescent emission of semiconductor and the commutable magnetic properties of magnetic nanoparticles. Magnetite is a non toxic magnetic nanomaterial which inducible magnetic moment allows their targeting to a defined location or to be heated with an external magnetic field (Tran and Webster 2010).

Further surface derivatization of such hybrid nanomaterials leaving pendant–SH groups are of importance for future work optimizing the use of silicon for targeting strategies in drug and gene delivery where the nanoparticles are attached to biomolecules through SH or NH organic groups (Lillo et al. 2015)(Caregnato et al. 2010).

Herein, we developed magnetite − PSi hybrids further derivatized by silanization to yield magnetic porous silicon with either −SiO− and −SH terminal groups and investigated the particles photoluminescence, singlet oxygen and superoxide anion radical generation in an attempt to evaluate the potential use of these particles as optical sensors and therapeutic agents in biological systems.

2. Materials and Methods

All reactants, standard equipment and detection methods used [High-resolution transmission electron microscopy (HRTEM), Atomic Force Microscopy (AFM), Magnetic Force Microscopy (MFM), X-ray photoelectron spectroscopy (XPS), Photoluminescence Measurements, Singlet Oxygen Phosphorescence Detection and Bilinear regression analysis] are described in the Supplementary Material (S.M. – Materials and S.M. – Characterization techniques, respectively).

Silicon Synthesis. Porous silicon colloidal particles were synthesized according to the methods published in the literature (Portoles et al. 2009).

The particles, which is referred as PSi, were left in the dark in the presence of air to obtain a mildly oxidized surface monolayer (Portoles et al. 2009).

Magnetite nanoparticles synthesis. They were prepared by coprecipitating a Fe^{2+}/Fe^{3+} mixed solution (the molar ratio Fe^{2+}: Fe^{3+} = 1:2) with a NH_4OH solution in air as reported in the literature (Thach, Hai, and Chau 2008). The concentration of Fe^{2+} used was 0.05 M, in order to obtain 10 nm sized nanoparticles. After the reaction, the dark precipitate of magnetite was washed several cycles with distilled water and magnetic decantation. These particles are named MNP.

Both toluene suspensions of PSi and MNP were prepared separately.

Hybrid Composites Preparation. A MNP suspension was added drop by drop at room temperature, to a PSi suspension under constant stirring, to a final concentration of 0.06 g/L MNP and 0.47 g/L PSi. The obtained solid was filtered with a 0.2 μm pore membrane and washed with toluene several times and finally suspended in toluene for further uses. These particles will be referred to as MPSi. As will be discussed further (vide *infra*), the maximum concentration of MNP used is limited to the observation of luminescence, see S.M.−PSi quenching.

Surface-Modification Procedures. To obtain PSi and MPSi with surface thiol groups, silanization reaction was performed employing MPTS which reacts with terminal Si−OH and Fe−OH present in surface oxidized PSi (Caregnato et al. 2010)(Caregnato, Dell 'Arciprete, and Gonzalez 2013) and magnetite environments (Li, He, and Swihart 2004)(Rosso-Vasic et al. 2008) (Yamaura et al. 2004)(Sundar, Mariappan, and Piraman 2014), respectively. To that purpose, the silane agent was added to suspended particles in toluene and stirred for 48 hours. The excess of MPTS was removed by membrane dialysis (Caregnato, Dell 'Arciprete, and Gonzalez 2013). Surface-modified samples were named PSi−SH and MPSi−SH, respectively.

3. Results and Discussion

3.1. Sample characterization

The XPS of PSi and MPSi (see Figure 1) shows the characteristic Si 2s, Si 2p, Fe 2p, and O 1s peaks.

PSi. The Si(2p) region displays the contribution of different environments for the silicon atoms. Peaks with a binding energy of 101.4, 102.2 and 103.6 eV with contributions of 15.4, 73.8 and 2.5%, respectively, were assigned to Si(–O–)x, where the coordination of oxygen is 2, 3 and 4. The peak at 98.8 eV was assigned to Si–Si with a contribution of 8.3% (Caregnato, Dell 'Arciprete, and Gonzalez 2013).

The O 1s peak contribution at 532.2 eV assigned to Si(O−)x environments, supports the oxidation of the silicon surface after storage ("NIST X-Ray Photoelectron Spectroscopy

Database, Version 4.1. National Institute of Standards and Technology: Gaithersburg, MD" 2012).

MPSi. Si(2p) and O(1s) region has the same peaks and contributions than PSi sample.

The Fe 2p XPS spectrum of MPSi includes two oxidation states, Fe(II) and Fe(III). The spectrum can be successfully fitted to four main peaks in the 2p3/2 region with a signal–separation, ΔBE(binding energy) (BE 2p3/2 − BE 2p1/2), of about 13.5 eV. The binding energy peak at 709 eV is attributed to Fe(II) compounds. Fe(III) octahedral species show BE of 711 eV and the Fe(III) tetrahedral species depict BE of 712.5 eV, in line with literature data for magnetite particles (Yamashita and Hayes 2008) (Wilson and Langell 2014). The lowest BE peak at 708.5 eV could be assigned to Si-O-Fe bridges, as was published by Bogatyrev and coworkers, for the Fe 2p XPS spectra of Fe_2O_3-SiO_2 nanocomposites (Bogatyrev et al. 2009).

The results of the deconvoluted peaks using the parameters defined above yield a Fe(II):Fe(III) ratio greater than the 0.5 expected for Fe_3O_4. This could be an indication of surface reduction under the ultrahigh vacuum conditions and X-ray flux of the measurement. However, as is reported in the literature (Wilson and Langell 2014), the satellite structure could be weakened in the nano-scaled material and cannot be meaningfully resolved into individual Fe(II) and Fe(III) components.
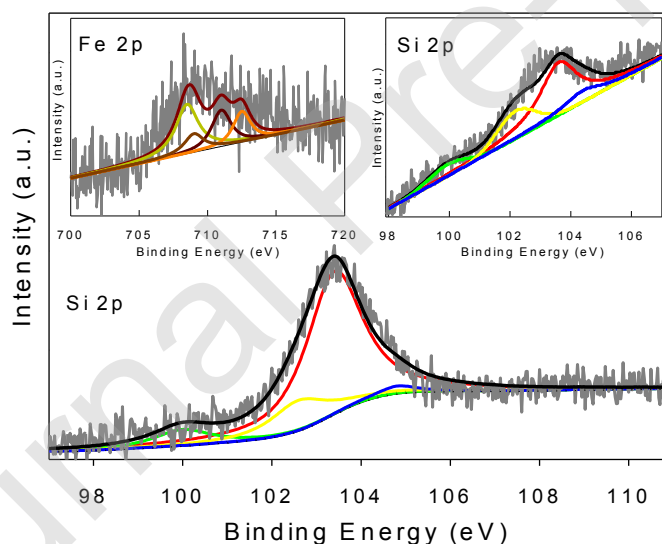

Figure 1. Main: XPS spectrum of the Si(2p) core level of the PSi sample. Insets: Si(2p) and Fe(2p) core levels of the MPSi sample.

AFM images were obtained for MNP, PSi and MPSi samples suspended in toluene, after dropcasting on a mica support and solvent evaporation.

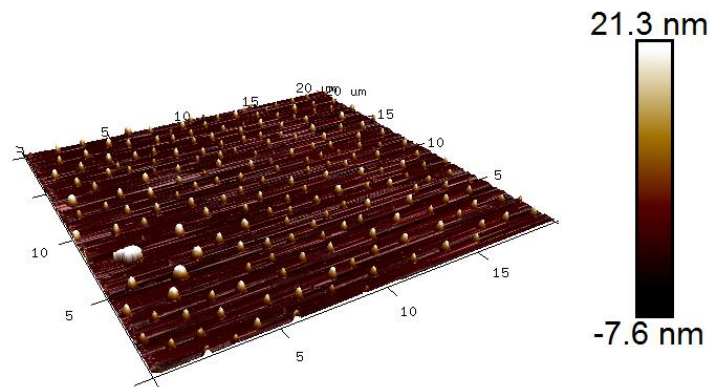From the corresponding AFM histogram of MNP, a mean particle height of (15 ± 5) nm is estimated (Figure 2).

Figure 2. Atomic force microscopy (AFM) 3D image MNP dropcast from toluene dispersion onto a mica substrate

Figure 3a and 3b show the AFM image of PSi and MPSi samples, respectively. The line scan profiles present the height information along the lines in the main picture. They show a step structure characteristic of porous particles. The height difference to the brighter point is about 130 nm (Figure 3b, 3c, and 3e).
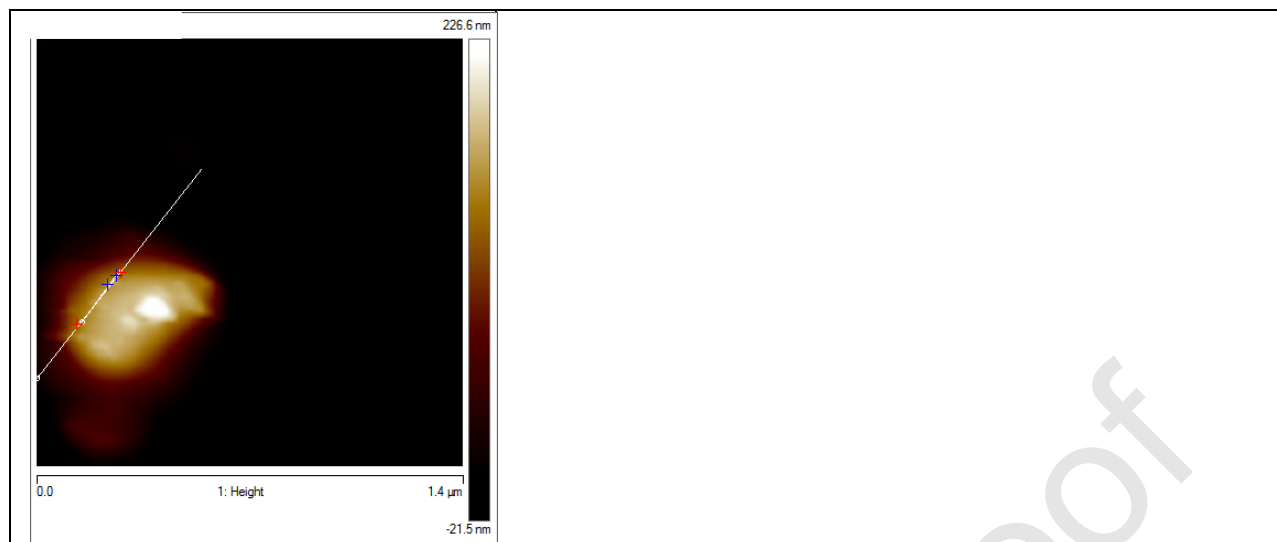

5
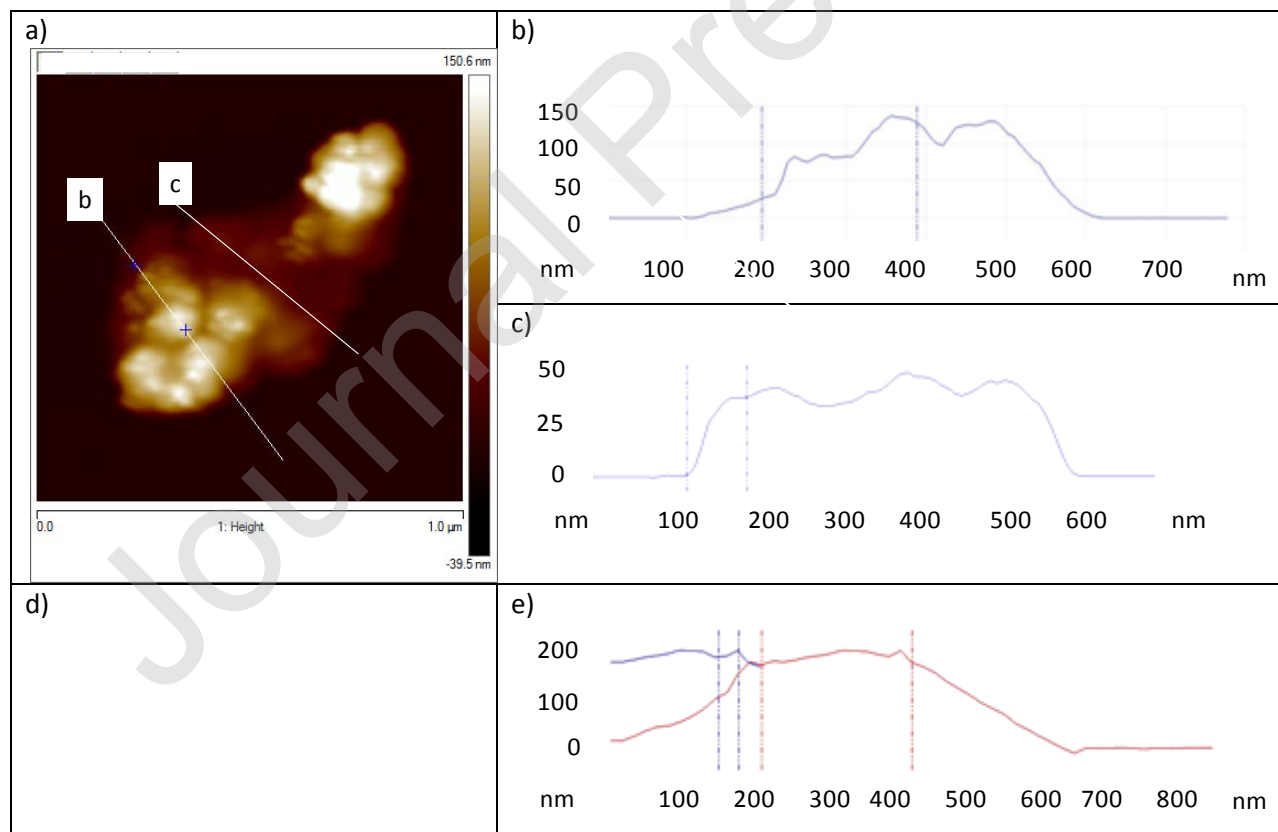
Figure 3. a)AFM image of PSi dropcast (a) and MPSi (d) from toluene dispersion onto a mica substrate (psi-15-11-2017.006) b) and c) line profiles analysis along the lines indicated in a), and e) line profile analysis along the lines indicated in d)

MFM characterization of MPSi particles is reported in Figure 4, which has been performed by acquiring the topography (Figure 4A) and the standard phase image during the first pass in tapping mode. The characterization of the same area has been repeated several times with different values of lift height Δz=0, 25, 50 and 100 nm (Figure 4B-D).

The phase's images from 0 to 100 nm show that the black intensity spots of face image, decreased with tip-sample distance, which confirms the magnetic property of the MPSi samples.

Similar measurements were taken for PSi samples which showed no magnetic properties. MFM images of Fe_2O_3 samples, showed dark areas in the phase image, which indicates magnetic interaction with the probe (See S.M.-Figure 2).

A)

300nm

-300nm

B)
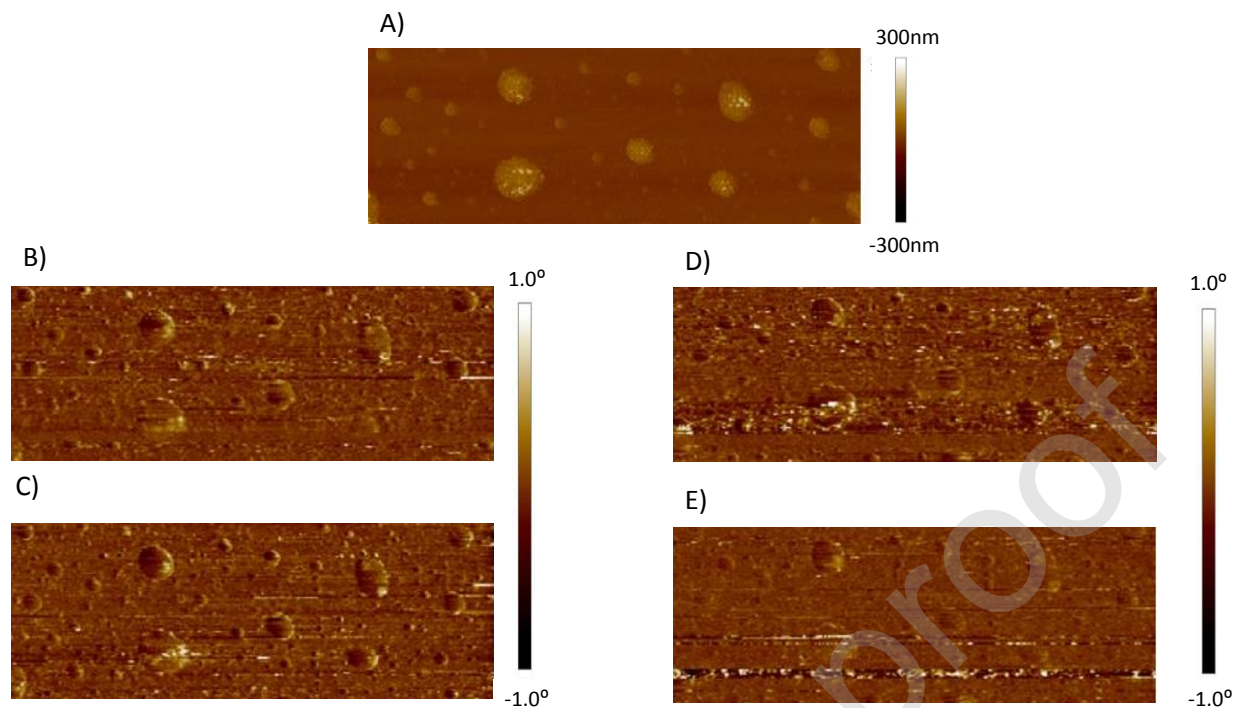
1.0°

D)

1.0°

C)

-1.0°

E)

-1.0°

Figure 4. MFM image MPSi dropcast from toluene dispersion onto a mica substrate. A) topography, B) phase $\Delta Z=0$ nm, C) phase $\Delta Z=25$ nm, D) phase $\Delta Z=50$ nm, E) phase $\Delta Z=100$ nm.

Representative HRTEM images for MNP (S.M.-Figure 3) and diffraction pattern indicate crystalline magnetite particles of ~10 nm size. Lattice spacing of 2.53 Å is consistent with the spacing of the (311) crystal plane of a face-centered cubic magnetite phase (Huang et al. 2012).

No diffraction pattern was found in TEM images of PSi samples, standing the amorphous structure of the porous silicon.

Figure 5 shows the HAADF-STEM images of PSi. The particles have an irregular shape characteristic of a porous structure, similar to AFM height profile described before.

TEM-EDS mapping profiles of PSi sample show the Si and O distribution, indicating that the silicon is surfaced oxidized (figure 5 b) and c)).

TEM image of MPSi can be seen in Figure 6a). HAADF-STEM and TEM-EDS pictures of the same region are shown in figure 6 b) and c). Mapping profiles indicate that Fe was mainly dispersed on the surface of silicon surrounding the PSi particles, and in smaller quantity it seems that Fe is inside de silicon structure. The mapping showing the oxygen distribution indicates that both iron and silicon nanoparticles are surface oxidized (Figure 6d)).

The TEM image in SI-Figure 3b) shows the same arrangement of MNP round the bigger silicon ones, confirming the crystallinity of the smaller 10 nm Fe_2O_3 ones.
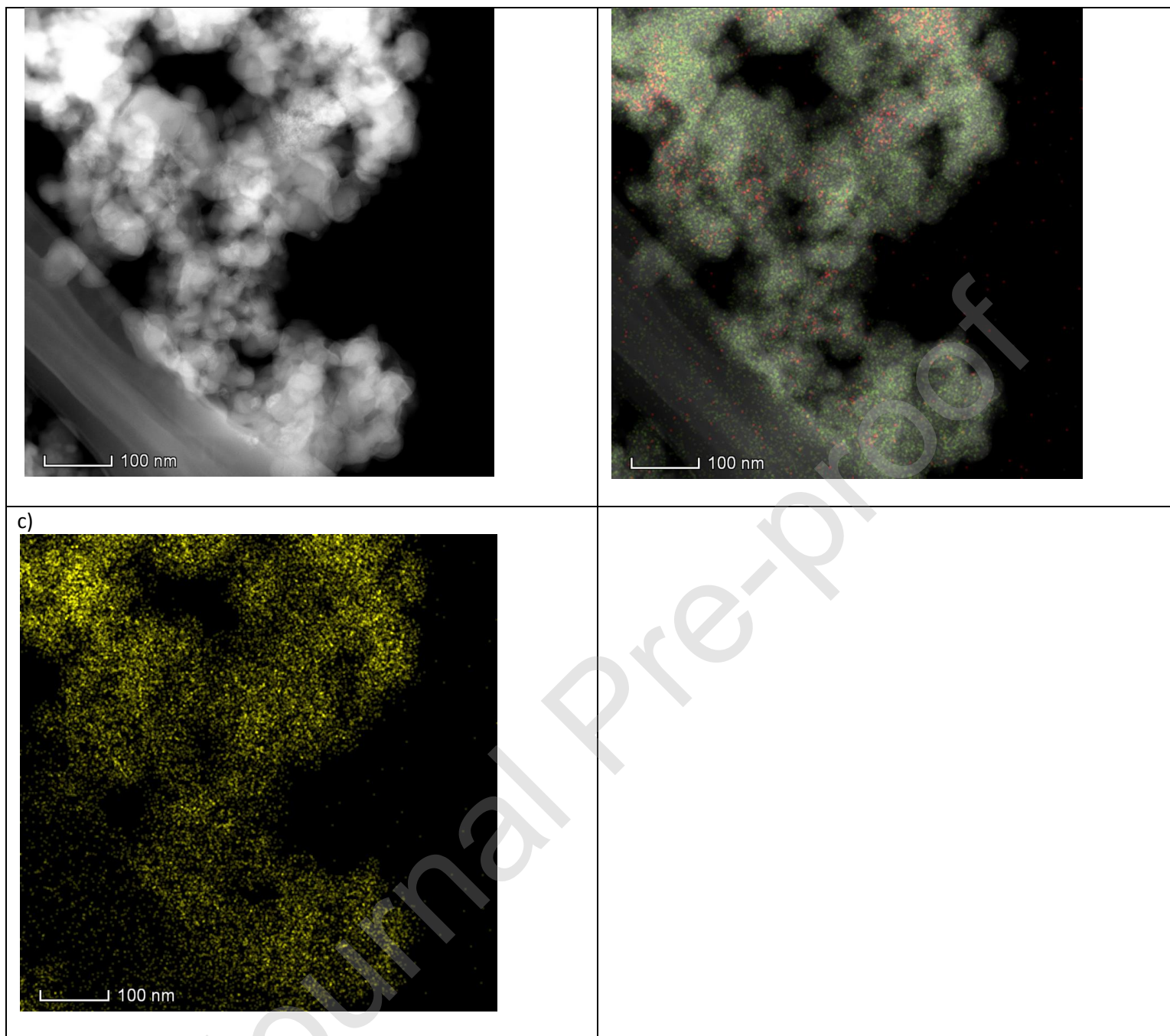
a)	b)

Figure 5. a) HAADF-STEM image of PSi sample. b) and c) TEM-EDS mapping profiles of PSi showing the Si (green) and O (yellow) distribution
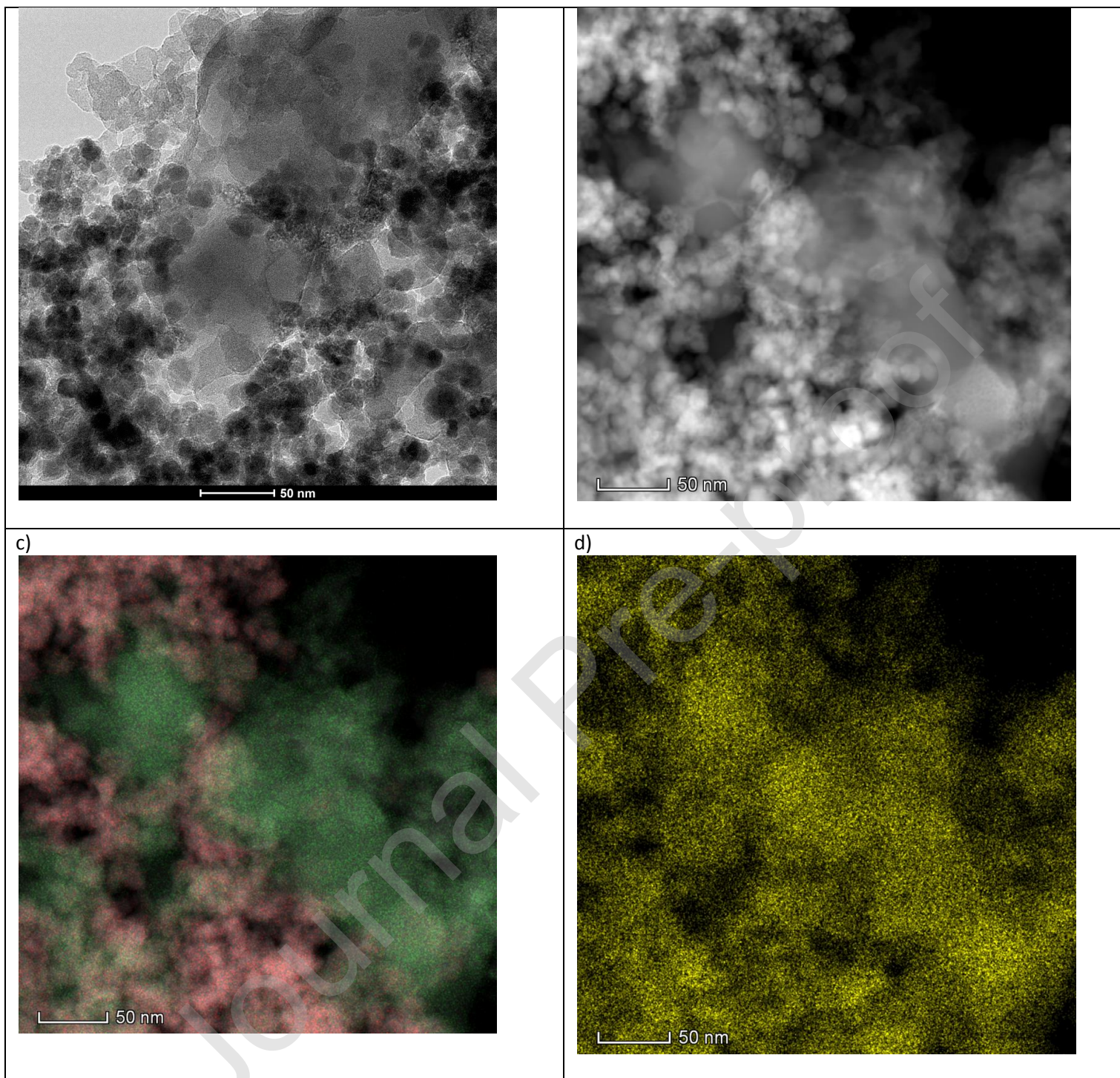
a)	b)

Figure 6. a) TEM image (a) and HAADF-STEM image (b) of MPSi sample. (c) and (d) TEM-EDS mapping profiles of MPSi showing the Si (green) and Fe (red) and O (yellow) distribution.

3.2. Photoluminescence experiments

9

Porous Silicon based materials have been reported to photoluminescence in the whole range of the visible region of the spectrum, and into the near UV. (Cullis, Canham, and Calcott 1997).

In our experiments, PSi shows PL in the wavelength range from 300 to 650 nm, with the emission spectrum strongly depending on the excitation wavelength in the specified range. Both, the incorporation of MNP and the surface derivatization with MPTS, introduce changes in PSi photoluminescence. A bilinear regression analysis of the emission–excitation matrix (E–EM) was performed in order to calculate the number of species and contribution of them to the overall E–EM. Moreover, the mean band gap energy of the species determined of each particles may be calculated from the excitation spectrum threshold of each individual species (Juan J. Romero et al. 2013) (Juan J. Romero et al. 2015). Obtained values are depicted in Table 1.

PSi suspensions in toluene show the contribution to the E–EM of a minimum of three species with an excitation–emission maximum at (λ_{exc}/nm, λ_{em}/nm): (290, 330), (330,370−420) and (285, 580) denoted as PSi1, PSi2 and PSi3, respectively (Figure 7a). Freshly prepared suspensions show higher PSi3 emission intensities than aged-suspensions. The intensity of the (285, 580) photoluminescence band diminishes when MNP toluene suspension is added dropwise to PSi (S.M. – PSi Quenching). No significant PL signal was observed for [MNP] ≥ 0.06g/L. In order to discard that an inner filter effect (IFEs) is the cause of the reduction of emission intensity at 580 nm, obtained luminescence data was corrected following literature recommendations (Juan José Romero et al. 2018) (S.M. – Luminescence intensity correction). Corrected fluorescence after removing the IFEs, probes that the quenching processes is mainly due to the presence of magnetite in the samples.

MPSi luminescence (see Figure 7b) may be described by two main contributing species with (λ_{exc}/nm, λ_{em}/nm): (290, 330) and (340, 380), denoted as MPSi1 and MPSi2, respectively. Emission at higher wavelengths is negligible under the experimental conditions used for obtaining EEM data.

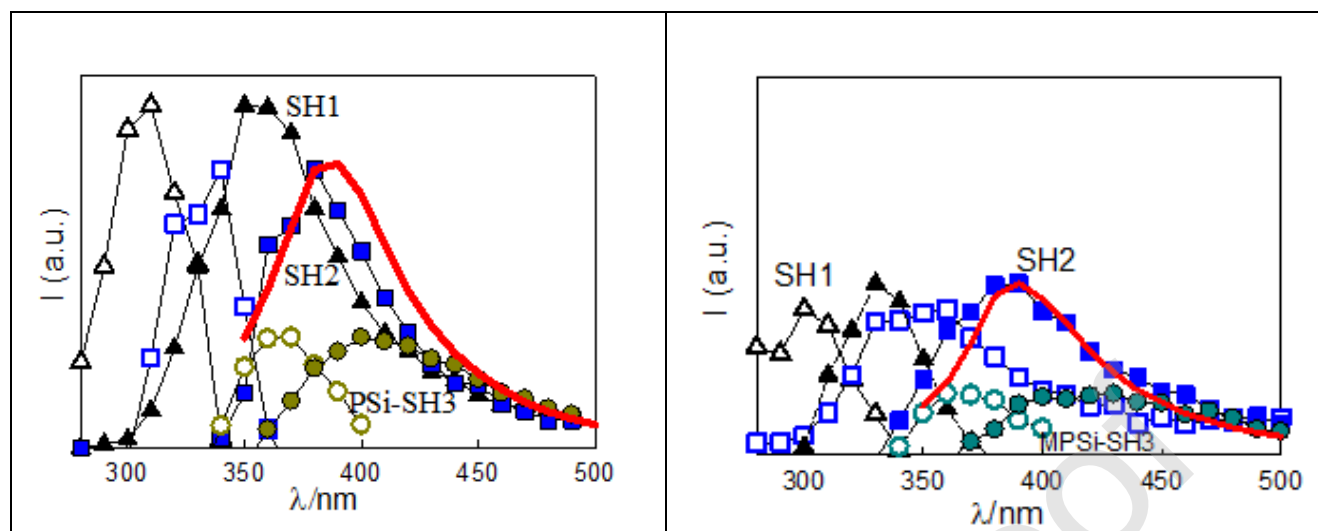a) PSi   b) MPSi   c) PSi-SH   d) MPSi-SH
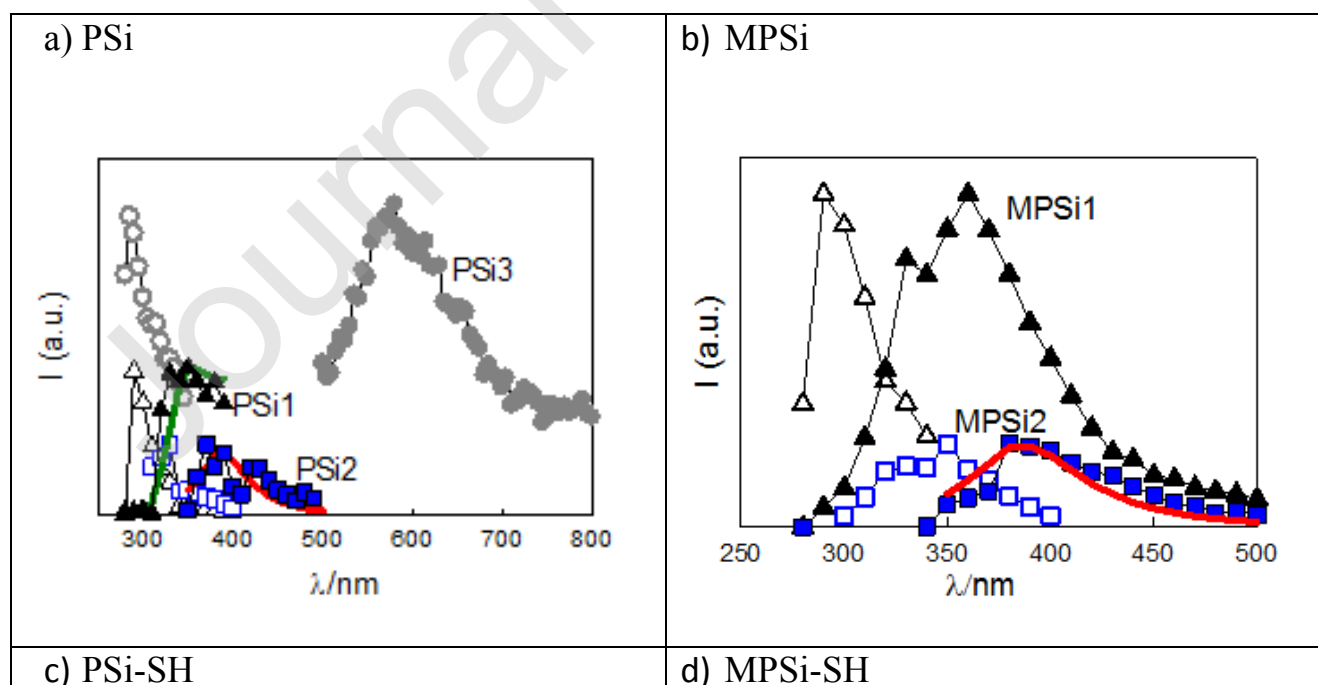
Figure 7. Excitation (open symbol) and emission (full symbol) spectra of the minimum number of contributing emitters to the overall PL as obtained from the bilinear analysis of the PL excitation−emission matrix of toluene suspensions of each PSi, MPSi, PSi-SH and MPSi-SH samples. Lines stands for the contribution to the overall emission due to the transient observed upon 298 (green) and 341 nm (red). Although the luminescence intensity is expressed in arbitrary units, it is in the same scale in all the figures.

The PL excitation−emission spectra, Energy gap (EG), λ^{em}_{max}, and Stokes Shift (SS) of emitting species PSi1 and MPSi1, are comparable within the experimental error and may therefore be assigned to the same contributing species (see Table 1). The EG values are coincident with the PL maximum and thus, confirm that the PL excitation and emission spectra of species PSi1 and MPSi1, originate from the same optical transitions. A similar situation is observed for emitting species PSi2 and MPSi2.

Table 1

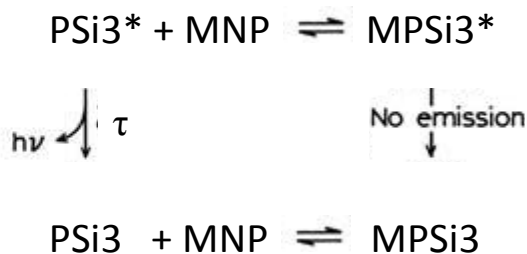| Fluorophore	E_{em}^{max}/eV	Energy Gap/eV	Stokes Shift /eV	τ/nsec.
PSi1	3.75 (330 nm)	3.63	0.51	8.32±0.05
PSi2	3.35 (370 nm)-2.95(420 nm)	2.95	0.41	9.28±0.1
PSi3	2.14 (580 nm)	2.2	2.21	*
MPSi1	3.75 (330 nm)	3.63	0.51	----
MPSi2	3.26 -3.1 (380-400 nm)	3.1	0.39	9.35±0.09
MPSiSH1	3.44 (360 nm)	3.62	0.69	----
MPSiSH2	3.26 (380 nm)	3.32	0.5	9.6±0.1
MPSiSH3	3.02 (410 nm)	2.92	0.42	----

*40 μs to 10 μs depending on emission wavelength

Table 1: Emision maximum (E_{em} ^{max}), Energy Gap, Stokes shift and luminescence decay times obtained for the different emitters of PSi, MPSi, and MPSiSH. Similar colors remark emitters corresponding to the same species.

The PL decay times, τ, of the different contributing species were obtained from exponential decay fittings of the PL traces obtained upon excitation at 295, 341 and 373 nm, respectively. Therefore, excitation at 295, 341, and 373 nm was performed to obtain τ values for PSi1, PSi2, and PSi3, respectively. Excitation of PSi in toluene suspensions at 295 and 341 nm lead to transient luminescence curves which could be well fitted to a monoexponential decay with decay times of (8.32±0.05) and (9.3±0.1) ns, respectively. The emission spectra of the two components resemble those obtained for PSi1 and PSi2 (see full colored lines in figure 7 a), confirming that PSi1 and PSi2 correspond to two well defined emitters contributing to the overall photoluminescence.

Time resolved experiments performed for MPSi in toluene suspensions yield, within the experimental error, similar τ and emission spectra to those observed for PSi1 and PSi2, further supporting our previous discussion suggesting that emitters PSi1 and MPSi1 correspond to the same species. A similar reasoning is valid for emitters PSi2 and MPSi2.

The presence of closely spaced and interconnected silicon nanocrystals of diameter < 5 nm may be responsible for PSi1 and PSi2 emitters, in line with literature reports on electrochemically etched PSi (Joo et al. 2016). In fact, small 2 nm size crystalline silicon nanoparticles (SiNp) show emission in the same region than PSi1 and PSi2 and similar PL lifetimes (Llansola Portoles et al. 2012) (Caregnato, Dell 'Arciprete, and Gonzalez 2013). Therefore, PSi1 and PSi2 emitters may be associated to silicon crystallites of 1-2 nm size, embedded within the PSi structure. Moreover, the luminescence of these crystallites is not affected by the presence of magnetite in MPSi samples. These crystallites are the main fluorophores observed in MPSi samples.

Spectra-LED excitation of PSi samples at 373 nm, leads to a PL decay that could be well fitted by a monoexponential function with lifetimes strongly depending upon the emission wavelength, with values decreasing from 40 μs at 650 nm to 10 μs at 500 nm (see figure 8). Similar results were found in literature indicating that room temperature decay times of PSi increase in a monotonic manner with increasing wavelength (Cullis, Canham, and Calcott 1997). Confinement effect, enhances the overlap between electron and hole wave functions, decreasing the radiative lifetimes at shortest wavelength (Bsiesy et al. 1991). Despite the emission intensity of MPSi in the wavelength range > 500 nm is much lower than that observed for PSi, it shows the same τ and wavelength dependence than PSi. As a consequence, it may be concluded that MNP quenching of the PL of PSi3 emitters involves a static process. According to our previous characterization of MPSi, MNP nanoparticles are either physically adsorbed or chemically bonded through Si-O-Fe bonds to the superficial silicon structure. The observed quenching of PSi3 photoluminescence by MNP is shown in scheme 1. It may be due to the creation of non-radiative surface states (MPSi3*) which are the superficial structural defects raised by MNP interaction with PSi (Kolasinski et al. 2000).

$$PSi3^* + MNP \rightleftharpoons MPSi3^*$$

$$h\nu \downarrow \tau \qquad \qquad \text{No emission} \downarrow$$

$$PSi3 + MNP \rightleftharpoons MPSi3$$

Scheme 1. Photoluminescence quenching mechanism proposed of MPSi nanoparticles.
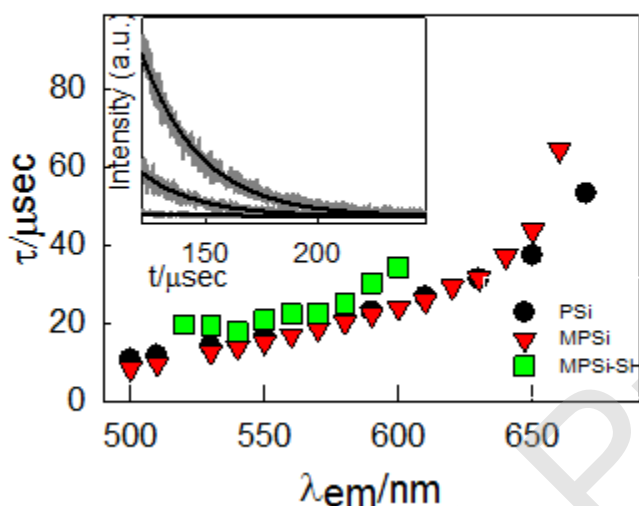

Figure 8. PL decay time after Spectra-LED excitation at 373nm vs emission wavelength for PSi, MPSi and MPSi-SH. Inset: Emission traces at 580nm after 373nm Spectra-LED excitation of particle toluene suspensions of PSi, MPSi and MPSi-SH (from top to bottom).

The emission−excitation spectra of both, PSi-SH and MPSi−SH, show the contribution of three emitting species. Those with (300, 360) and (330, 380) (see Figure 7c and 7d), named consecutively as SH1 and SH2 are identical, though their luminescence intensity diminish when MPSi surface is derivatized with MPTS to yield MPSi-SH. The third emitter observed at (λ_{exc}/nm, λ_{em}/nm): (360, 410) for MPSi−SH and at (370, 400) for PSi-SH have no correlation with those observed for MPSi and PSi. The appearance of this new emitter is in line with reported studies (Caregnato, Dell 'Arciprete, and Gonzalez 2013) describing that surface modification of silicon nanoparticles with thiol organic groups, which brings in a new contributing species to the excitation-emission matrix with (λ_{exc}/nm, λ_{em}/nm):(370, 410−430).
Spectra-LED excitation of PSi-SH samples at 373 nm, leads to a PL decay that could be well fitted by a monoexponential function with lifetimes strongly depending upon the emission wavelength, as described before and also shown in figure 8. Observed τ values and wavelength dependence are similar to those of PSi3 emitters, thus also supporting a static quenching of PSi3 by organic chemisorbed molecules. A unique excitation transition leading to exciton formation

and its further relaxation to different lower-lying emitting states originated from different surface defects introduced by S, O, and Fe is also inferred.

3.3. ROS generation

Singlet oxygen ($^1O_2$) formation upon 355 nm and 266 nm irradiation of PSi and MPSi in acetonitrile suspensions is evidenced by the time-resolved phosphorescence traces observed at 1270 nm. $^1O_2$ traces were fitted to an exponential decay law according to the equation: $I^1O_2(t) = I^1O_2(t=0) \times \exp(-t/\tau_\Delta)$ with I the phosphorescence intensity (see fitting curves in Figure 9) and τ_Δ the $^1O_2$ lifetime.

Obtained singlet oxygen quantum yields, Φ_Δ, are shown in Table 2. Values of 0.26 and 0.08 were obtained for PSi and MPSi. Φ_Δ value obtained for MPSi is on the order of that published in the literature for iron containing 2 nm silicon nanoparticles after 355 nm irradiation ($\Phi_\Delta = 0.06\pm0.01$) (Juan J. Romero et al. 2015).

Singlet oxygen lifetimes (see Table 2), obtained from the decay of phenalenone traces are in agreement with literature data (Darmanyan and Foote 1993). Singlet oxygen lifetimes calculated in suspensions of PSi and MPSi (see traces in Figure 9 and Table 2) are smaller than τ_Δ obtained for the references, indicating a possible reaction between $^1O_2$ generated and the particles surface. The τ_Δ value of MPSi, is slightly smaller than that of iron-free surface-oxidized PSi, showing a small effect of iron on $^1O_2$ reactivity.

It is interesting to note that, MNP is able to efficiently quench the $^1O_2$ produced by a reference in acetonitrile but does not affect singlet oxygen lifetime (S.M.–Figure 4). Therefore, MNP does not undergo neither dynamical physical, nor chemical interactions with $^1O_2$. However, this is not the case of $^1O_2$ reaction with MPSi, where a dynamic quenching contribution is also observed. This could be due to differences with surface groups present in PSi and MPSi. Surface Si-O-Fe groups present in MPSi interact with $^1O_2$ in a different way that Si-O-Si in PSi surface do.

Table 2

	Phenalenone	PSi	MPSi
Φ_Δ (acetonitrile) $\lambda_{exc.}$ 266 nm	0.95	0.26 ± 0.01	0.08 ± 0.01
Φ_Δ (acetonitrile) $\lambda_{exc.}$ 355 nm	0.95	0.27±0.05	----*----
τ_Δ (acetonitrile, $\lambda_{exc.}$ 266 nm)/µs	66.6 ± 0.2	57.1 ± 0.2	53.3 ± 0.4
[H_2O_2] at $\lambda_{exc.}$ 350 nm	---------	2.9×10^{-4}M	8.1×10^{-5}M

* Singlet oxygen traces too small for performing calculations.

Table 2. Singlet oxygen quantum yields (Φ_Δ) and decay times (τ_Δ)

Since Superoxide radical anion ($O_2^{\bullet-}$) recombination leads to H_2O_2 production, a commercial enzymatic colorimetric assay was used to measure [H_2O_2] as an indirect method (Lillo et al. 2015) for determining $O_2^{\bullet-}$ generation. H_2O_2 formation was observed in irradiation experiments of PSi and MPSi aqueous suspensions at $\lambda_{exc.}$ 350 nm, concluding that both samples generate $O_2^{\bullet-}$. However, MPSi is a poorer source of $O_2^{\bullet-}$ than PSi.
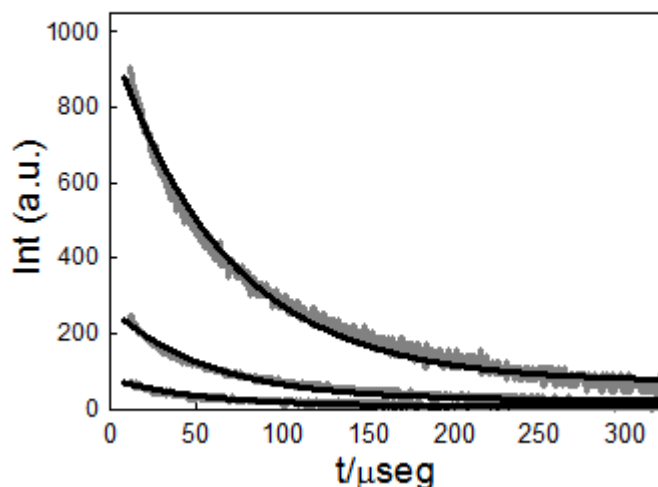
Figure 9. Singlet oxygen phosphorescence decay curves at 1270 nm obtained upon 266 nm excitation of samples in air-saturated acetonitrile solution. From top to button: reference (phenalenone), PSi and MPSi. Black lines stand for the curves fitting to a single exponential decay.

According to the results exposed, the only specie that absorbs at 266 nm in PSi sample, is PSi3. MNPs are mainly distributed in the outer surface of PSi, quenching statically the visible PL and $^1O_2$ production.

This means that PSi3 is associated with surface excited states of porous silicon. PL of this specie is also statically quenched by MPTS in PSi–SH samples (vide supra).

Upon 355 nm irradiation of PSi, the $^1O_2$ quantum yield production is (0.27±0.05), supporting the fact that PSi3 is the specie responsible of $^1O_2$ production.

The specie PSi3 has an energy gap ~ 2 eV and a lifetime in the order of microseconds. Goller and coworkers have demonstrated that excitons having these energies and lifetimes, efficiently undergo an energy transfer to oxygen molecules physisorbed on the surface of silicon nanoparticles, generating $^1O_2$ (Goller et al. 2010).

Superoxide radical anion ($O_2^{\bullet-}$) production occurs via a charge transfer of exitons to molecular oxygen, as it was demonstrated in previous reports (Lillo et al. 2015).

In conclusion, the exposed surface of PSi is very sensitive to the presence of adsorbed molecules or small particles to the optical properties and ROS generation of the material.

Myndrul and co workers have published that gold coated porous silicon nanocomposite, which has a PL peak in the same visible spectra region than the bared PSi, showed that the PL intensity of PSi-Au materials diminishes gradually with the increase of the thickness of Au layer (Myndrul et al. 2017).

In addition, the use of PSi-based photoluminescence immunosensors, shows a quenching of the visible PL with the increase of the target molecule adsorbed to the receptors chemically modified PSi surface (Myndrul et al. 2018).

This means that, 10 nm magnetite nanoparticles, are not able to reach the internal pores of MPSi, and do not modify the nanocrystalline silicon network and smaller pores volume distribution, which are responsible for the PL in the UV region of spectra (PSi1 and PSi2 species).

4. Conclusions

Magnetic porous silicon nanoparticles were obtained by suspending 10-15 nm diameter of magnetite nanoparticles into porous silicon suspensions. Fe-containing PSi quenches the visible luminescence at $\sim$ 580 nm characteristic of porous silicon by a static process. Nevertheless, these particles have $^1O_2$ photosensitizing properties, stable luminescence in the range 330-400 nm, and produce $O_2^{\cdot-}$, which make them important candidates for biomedical applications.

Declaration of interests
The authors declare that they have no known competing financial interests or personal relationships that could have appeared to influence the work reported in this paper.

CRediT author statement
Paula Caregnato: experimental work, data analysis and conclusions, Writing- Original draft preparation, Reviewing and Editing.
Pedro M. David Gara: ROS measurementsn analysis and conclusions, Reviewing and Editing
Eduardo D. Prieto: Microscopy (AFM and MFM) measurements, anlysis, and conclusions.
Mónica C. Gonzalez: Supervision, Reviewing and Editing.

References

Airaksinen, Anu J, Hélder A Santos, Ermei Mäkilä, Jouni Hirvonen, and Luis M Bimbo. 2014. "Porous Silicon Nanoparticles for Nanomedicine: Preparation and Biomedical Applications." *Nanomedicine* 9 (4): 535–54. https://doi.org/10.2217/nnm.13.223.

Bogatyrev, V. M., V. M. Gun'ko, M. V. Galaburda, M. V. Borysenko, V. A. Pokrovskiy, O. I. Oranska, E. V. Polshin, O. M. Korduban, R. Leboda, and J. Skubiszewska-Zieba. 2009. "Synthesis and Characterization of Fe2O3/SiO2nanocomposites." *Journal of Colloid and Interface Science* 338 (2): 376–88. https://doi.org/10.1016/j.jcis.2009.06.044.

Bsiesy, A., J. C. Vial, F. Gaspard, R. Herino, M. Ligeon, F. Muller, R. Romestain, A. Wasiela, A. Halimaoui, and G. Bomchil. 1991. "Photoluminescence of High Porosity and of Electrochemically Oxidized Porous Silicon Layers." *Surface Science* 254 (1–3): 195–200. https://doi.org/10.1016/0039-6028(91)90652-9.

Caregnato, Paula, Maria Laura Dell 'Arciprete, and Mónica Cristina Gonzalez. 2013. "Silanization Effect on the Photoluminescence Characteristics of Crystalline and Amorphous Silicon Nanoparticles." *Photochem. Photobiol. Sci* 12 (9): 1658–1655. https://doi.org/10.1039/c3pp50067e.

Caregnato, Paula, Malcolm D E Forbes, Delia B Soria, Daniel O Mártire, and Mónica C Gonzalez. 2010. "Chemisorbed Thiols on Silica Particles: Characterization of Reactive Sulfur Species." *J. Phys. Chem. C* 114 (11): 5080–5087. https://doi.org/10.1021/jp911253f.

Cullis, A. G., L. T. Canham, and P. D.J. Calcott. 1997. "The Structural and Luminescence Properties of Porous Silicon." *Journal of Applied Physics* 82 (3): 909–65. https://doi.org/10.1063/1.366536.

Darmanyan, Alexander P., and Christopher S. Foote. 1993. "Solvent Effects on Singlet Oxygen Yield from n,.Pi.* and .Pi.,.Pi.* Triplet Carbonyl Compounds." *Journal of Physical Chemistry* 97 (19): 5032–35. https://doi.org/10.1021/j100121a029.

Goller, B., S. Polisski, H. Wiggers, and D. Kovalev. 2010. "Silicon Nanocrystals Dispersed in Water: Photosensitizers for Molecular Oxygen." *Applied Physics Letters* 96 (21): 19–22. https://doi.org/10.1063/1.3432349.

Huang, Xiaodan, Xufeng Zhou, Kun Qian, Dongyuan Zhao, Zhaoping Liu, and Chengzhong Yu. 2012. "A Magnetite Nanocrystal/Graphene Composite as High Performance Anode for Lithium-Ion Batteries." *Journal of Alloys and Compounds* 514: 76–80. https://doi.org/10.1016/j.jallcom.2011.10.087.

Joo, Jinmyoung, Thomas Defforge, Armando Loni, Dokyoung Kim, Z. Y. Li, Michael J. Sailor, Gael Gautier, and Leigh T. Canham. 2016. "Enhanced Quantum Yield of Photoluminescent Porous Silicon Prepared by Supercritical Drying." *Applied Physics Letters* 108 (15). https://doi.org/10.1063/1.4947084.

Kolasinski, Kurt W., John C. Barnard, Santanu Ganguly, Lynne Koker, Anja Wellner, Mark Aindow, Richard E. Palmer, Christian N. Field, Paul A. Hamley, and Martyn Poliakoff. 2000. "On the Role of the Pore Filling Medium in Photoluminescence from Photochemically Etched Porous Silicon." *Journal of Applied Physics* 88 (5): 2472–79. https://doi.org/10.1063/1.1287770.

Li, Xuegeng, Yuanqing He, and Mark T Swihart. 2004. "Surface Functionalization of Silicon Nanoparticles Produced by Laser-Driven Pyrolysis of Silane Followed by HF- HNO3 Etching." *Langmuir* 20 (11): 4720–27.

Lillo, Cristian R, Juan J Romero, Manuel Llansola Portolés, Reinaldo Pis Diez, Paula Caregnato, and Mónica C Gonzalez. 2015. "Organic Coating of 1–2-Nm-Size Silicon Nanoparticles: Effect on Particle Properties." *Nano Research* 8 (6): 2047–62. https://doi.org/10.1007/s12274-015-0716-z.

Llansola Portoles, Manuel J, Reinaldo Pis Diez, María L Dell 'arciprete, Paula Caregnato, Juan Joseomero, Daniel O Matire, Omar Azzaroni, Marcelo Ceolín, and Moica C Gonzalez. 2012. "Understanding the Parameters Affecting the Photoluminescence of Silicon Nanoparticles." *J. Phys. Chem. C* 116 (20): 11315−11325. https://doi.org/10.1021/jp2117938.

Martin-Palma, Raul J. 2010. "Biomedical Applications of Nanostructured Porous Silicon: A Review." *Journal of Nanophotonics* 4 (1): 042502. https://doi.org/10.1117/1.3496303.

Myndrul, Valerii, Roman Viter, Maryna Savchuk, Maryna Koval, Nikolay Starodub, Viesturs Silamiķelis, Valentyn Smyntyna, Arunas Ramanavicius, and Igor Iatsunskyi. 2017. "Gold Coated Porous Silicon Nanocomposite as a Substrate for Photoluminescence-Based Immunosensor Suitable for the Determination of Aflatoxin B1." *Talanta* 175 (July): 297–304. https://doi.org/10.1016/j.talanta.2017.07.054.

Myndrul, Valerii, Roman Viter, Maryna Savchuk, Nelya Shpyrka, Donats Erts, Daniels Jevdokimovs, Viesturs Silamiķelis, Valentyn Smyntyna, Arunas Ramanavicius, and Igor Iatsunskyi. 2018. "Porous Silicon Based Photoluminescence Immunosensor for Rapid and Highly-Sensitive Detection of Ochratoxin A." *Biosensors and Bioelectronics* 102 (November 2017): 661–67. https://doi.org/10.1016/j.bios.2017.11.048.

"NIST X-Ray Photoelectron Spectroscopy Database, Version 4.1. National Institute of Standards and Technology: Gaithersburg, MD." 2012. 2012. http://srdata.nist.gov/xps/.

Portoles, M J, F R Nieto, D B Soria, J I Amalvy, P J Peruzzo, D O Martire, M Kotler, O Holub, and M C Gonzalez. 2009. "Photophysical Properties of Blue - Emitting Silicon Nanoparticles." *J Phys Chem C Nanomater Interfaces* 113 (31): 13694–702. https://doi.org/10.1021/jp903727n.

Romero, Juan J., Manuel J. Llansola-Portolés, María Laura Dell'Arciprete, Hernán B. Rodríguez, Ana L. Moore, and Mónica C. Gonzalez. 2013. "Photoluminescent 1-2 Nm Sized Silicon Nanoparticles: A Surface-Dependent System." *Chemistry of Materials* 25 (17): 3488–98. https://doi.org/10.1021/cm401666a.

Romero, Juan J., Marc Wegmann, Hernán B. Rodríguez, Cristian Lillo, Aldo Rubert, Stefanie Klein, Mónica L. Kotler, Carola Kryschi, and Mónica C. Gonzalez. 2015. "Impact of Iron Incorporation on 2-4 Nm Size Silicon Nanoparticles Properties." *Journal of Physical Chemistry C* 119 (10): 5739–46. https://doi.org/10.1021/acs.jpcc.5b00172.

Romero, Juan José, José H. Hodak, Hernán B. Rodríguez, and Mónica C. Gonzalez. 2018. "Silicon Quantum Dots Metal-Enhanced Photoluminescence by Gold Nanoparticles in Colloidal Ensembles: Effect of Surface Coating." *Journal of Physical Chemistry C* 122 (47): 26865–75. https://doi.org/10.1021/acs.jpcc.8b09310.

Rosso-Vasic, Milena, Evan Spruijt, Barend Van Lagen, Luisa De Cola, and Han Zuilhof. 2008. "Alkyl-Functionalized Oxide-Free Silicon Nanoparticles: Synthesis and Optical Properties." *Small* 4 (10): 1835–41. https://doi.org/10.1002/smll.200800066.

Sundar, Sasikala, Ramalakshmi Mariappan, and Shakkthivel Piraman. 2014. "Synthesis and Characterization of Amine Modified Magnetite Nanoparticles as Carriers of Curcumin-Anticancer Drug." *Powder Technology* 266: 321–28. https://doi.org/10.1016/j.powtec.2014.06.033.

Thach, C. V., N. H. Hai, and N. Chau. 2008. "Size Controlled Magnetite Nanoparticles and Their Drug Loading Ability." *Journal of the Korean Physical Society* 52 (5): 1332. https://doi.org/10.3938/jkps.52.1332.

Tran, Nhiem, and Thomas J. Webster. 2010. "Magnetic Nanoparticles: Biomedical Applications and Challenges." *Journal of Materials Chemistry* 20 (40): 8760–67. https://doi.org/10.1039/c0jm00994f.

Wilson, D., and M. A. Langell. 2014. "XPS Analysis of Oleylamine/Oleic Acid Capped Fe3O4nanoparticles as a Function of Temperature." *Applied Surface Science* 303: 6–13. https://doi.org/10.1016/j.apsusc.2014.02.006.

Yamashita, Toru, and Peter Hayes. 2008. "Analysis of XPS Spectra of Fe2+ and Fe3+ Ions in Oxide Materials." *Applied Surface Science* 254 (8): 2441–49. https://doi.org/10.1016/j.apsusc.2007.09.063.

Yamaura, M., R. L. Camilo, L. C. Sampaio, M. A. Macêdo, M. Nakamura, and H. E. Toma. 2004. "Preparation and Characterization of (3-Aminopropyl)Triethoxysilane-Coated Magnetite Nanoparticles." *Journal of Magnetism and Magnetic Materials* 279 (2–3): 210–17. https://doi.org/10.1016/j.jmmm.2004.01.094.